Carbenes Hot Paper

How to cite: *Angew. Chem. Int. Ed.* **2023,** *62,* e202215244
International Edition: doi.org/10.1002/anie.202215244
German Edition: doi.org/10.1002/ange.202215244

Crystalline Anions Based on Classical N-Heterocyclic Carbenes

Arne Merschel[+], Dennis Rottschäfer[+], Beate Neumann, Hans-Georg Stammler, Mark Ringenberg, Maurice van Gastel, T. Ilgin Demirer, Diego M. Andrada, and Rajendra S. Ghadwal**

Dedicated to Professor Guy Bertrand on the occasion of his 70th birthday.

Abstract: Herein, the first stable anions K[SIPr^{Bp}] (**4a-K**) and K[IPr^{Bp}] (**4b-K**) (SIPr^{Bp} = BpC{N(Dipp)CH$_2$}$_2$, IPr^{Bp} = BpC{N(Dipp)CH}$_2$; Bp = 4-PhC$_6$H$_4$; Dipp = 2,6-*i*Pr$_2$C$_6$H$_3$) derived from classical N-heterocyclic carbenes (NHCs) (i.e. SIPr and IPr) have been isolated as violet crystalline solids. **4a-K** and **4b-K** are prepared by KC_8 reduction of the neutral radicals [SIPr^{Bp}] (**3a**) and [IPr^{Bp}] (**3b**), respectively. The radicals **3a** and **3b** as well as [Me-IPr^{Bp}] **3c** (Me-IPr^{Bp} = BpC{N(Dipp)CMe}$_2$) are accessible as crystalline solids on treatment of the respective 1,3-imidazoli(ni)um bromides (SIPr^{Bp})Br (**2a**), (IPr^{Bp})Br (**2b**), and (Me–IPr^{Bp})Br (**2c**) with KC_8. The cyclic voltammograms of **2a–2c** exhibit two one-electron reversible redox processes in −0.5 to −2.5 V region that correspond to the radicals **3a–3c** and the anions (**4a–4c**)$^-$. Computational calculations suggest a closed-shell singlet ground state for (**4a–4c**)$^-$ with the singlet-triplet energy gap of 17–24 kcal mol^{-1}.

Introduction

Organic molecules exhibiting readily accessible multiple redox-states are highly sought-after species in materials science on account of their applications in data[1] and energy[2] storage as well as in logic operations suitable for quantum information science.[3] In this context, stable organic radicals and diradicals are of a particular significance as molecular building-blocks for optoelectronic[4] and other energy related materials.[5] This is because of their open-shell electronic structures, giving rise to interesting electronic, magnetic, and optical properties.[6] Radicals are well-known reactive intermediates in organic chemistry, and in general highly reactive.[7] The first stable radical, the so-called trityl radical Ph_3C, was isolated by Gomberg in 1900.[8] Currently, a variety of stable radicals are known, but most of them are based on a redox-active (N, O, and S in particular) heteroatom.[9] Thus, the number of stable carbon-centered radicals remained rather limited.[9,10]

Over the past years, stable singlet carbenes (i.e. N-heterocyclic carbenes, NHCs; cyclic alkyl amino carbenes, cAACs) have been intensively explored for deriving stable organic as well as main-group radicals.[11] Classical NHCs **II** (Scheme 1) are usually prepared by the deprotonation of 1,3-imidazoli(ni)um salts (**I-H**), which may formally be regarded as a two-electron reduction process. One electron-reduction products of **I-H** would be radicals, e. g., **III-H**. Already in 2004, Clyburne et al. probed the synthetic viability of an NHC-radical **III-H** (R = Mes = 2,4,6-Me$_3$C$_6$H$_3$) by the reduction of **I-H** with potassium in boiling THF. **III-H** was found to be unstable and decomposed into the free NHC (**II**) and, presumably, hydrogen.[12] This finding indicates the inappropriateness of hydrogen at the C2-position of NHCs in accessing stable radicals. In 2015, we reported the direct C2-arylation of NHCs by means of

[*] A. Merschel,[+] Dr. D. Rottschäfer,[+] B. Neumann, Dr. H.-G. Stammler, Priv.-Doz. Dr. R. S. Ghadwal
Anorganische Molekülchemie und Katalyse, Lehrstuhl für Anorganische Chemie und Strukturchemie, Centrum für Molekulare Materialien, Fakultät für Chemie, Universität Bielefeld
Universitätsstr. 25, 33615 Bielefeld (Germany)
E-mail: rghadwal@uni-bielefeld.de
Homepage: https://www.ghadwalgroup.de

Dr. M. Ringenberg
Institut für Anorganische Chemie, Universität Stuttgart
Pfaffenwaldring 55, 70569 Stuttgart (Germany)

Dr. M. van Gastel
Max-Planck-Institut für Kohlenforschung
Kaiser-Wilhelm-Platz 1, 45470 Mülheim a.d. Ruhr (Germany)

T. I. Demirer, Dr. D. M. Andrada
Allgemeine und Anorganische Chemie, Universität des Saarlandes
66123 Saarbrücken (Germany)
E-mail: diego.andrada@uni-saarland.de

Dr. D. Rottschäfer[+]
Current address: Department of Chemistry, Philipps-University Marburg
Hans-Meerwein-Str. 4, Marburg (Germany)

[+] These authors contributed equally to this work.

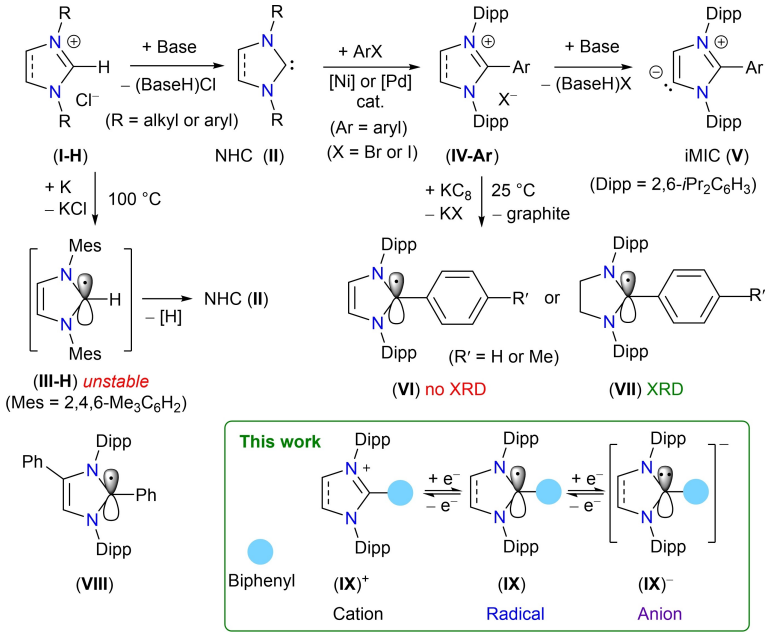

Scheme 1. Classical NHC precursors (**I-H**), NHCs (**II**), a putative NHC-radical (**III-H**). iMIC-precursors (**IV-Ar**), iMICs (**V**), and stable radicals (**VI**, **VII**, **VIII**). Stable radicals (**IX**) and anions $(\mathbf{IX})^-$ derived from C2-biphenylated 1,3-imidazoli(ni)um cations $(\mathbf{IX})^+$.

palladium catalysis to access C2-arylated 1,3-imidazol(ni)um salts **IV-Ar**,[13] which proved to be appropriate precursors for the synthesis of C5-protonated mesoionic carbenes (iMICs) **V** and related metal complexes.[14] Unlike **I-H**, the cyclovoltammograms (CVs) of **IV-Ar** show a reversible one-electron (1e) reduction process that corresponds to the neutral radical species. In 2018, we reported the crystalline radicals **VI** and **VII** by KC_8 reduction of **IV-Ar**.[15] Of note, C2-arylated NHC-radicals were previously proposed as intermediates in the n-type doping of organic thin film transistors.[16] The stability of **VI** and **VII** is mainly attributed to the delocalization of the unpaired electron over the C2-aryl substituent. Later, the radical **VIII** based on Bertrand's tetraarylated 1,3-imidazole was also reported.[17] With a suitable reagent, radicals **VI** and **VII** can be easily oxidized back to the corresponding precursors **IV-Ar**, which is consistent with their CVs. In principle, 1e-reduction of **VI** and **VII** would lead to the corresponding anions $(\mathbf{VI/VII})^-$, introducing an additional redox state to the systems. However, the absence of a related redox wave in the CVs of **IV-Ar** rules out this feasibility. Indeed, no reaction was observed on treatment of **VI** and **VII** with KC_8. Unlike **VII**, radicals based on unsaturated NHCs such as **VI** showed limited stability in solutions and could not be characterized by single crystal X-ray diffraction (sc-XRD).[15]

To further examine the impact of the C2-substituent on the stability and properties of radicals,[18] we sought to prepare new salts featuring a larger aryl substituent at the C2-position of NHCs. Herein, we describe the synthesis of crystalline radicals **IX** as well as anions $(\mathbf{IX})^-$ by the sequential 1e-reduction of the corresponding C2-biphenylated 1,3-imidazoli(ni)um cations $(\mathbf{IX})^+$. Notably, the use of a biphenyl substituent at the C2-position of NHCs not only lowers the reduction potential of $(\mathbf{IX})^+$ (cf. **IV-Ar**) to give the radicals **IX** but also brings in an additional stable redox state (i.e. the anions). The isolation of the anions $(\mathbf{IX})^-$ is unprecedented in the NHC chemistry.

Results and Discussion

The desired 1,3-imidazoli(ni)um bromides ($SIPr^{Bp}$)Br (**2a**), (IPr^{Bp})Br (**2b**),[14d] and (Me-IPr^{Bp})Br (**2c**) ($SIPr^{Bp}$ = BpC{N-(Dipp)CH_2}$_2$, IPr^{Bp} = BpC{N(Dipp)CH}$_2$, Me-IPr = BpC{N-(Dipp)CMe}$_2$; Bp = 4-PhC_6H_4; Dipp = 2,6-*i*Pr$_2$C$_6$H$_3$) were prepared by the direct C2-arylation of the corresponding NHCs (SIPr (**1a**), IPr (**1b**), and Me-IPr (**1c**)) with 4-bromobiphenyl (BpBr) using nickel catalysis as originally developed by this laboratory (Figure 1a).[14b] **2a**, **2b**, and **2c** are colorless air-stable solids and exhibit expected ^{1}H and ^{13}C NMR signals. The ^{1}H NMR spectra of **2a**–**2c** each exhibit two doublets and one septet for the isopropyl groups. The 1,3-imidazolinium back-bone protons (CH_2) of **2a** appear as a singlet at 4.58 ppm in the ^{1}H NMR spectrum. The ^{13}C{^{1}H} NMR spectrum of **2a** exhibits resonances for the Dipp and Bp groups, which can be appropriately assigned to the carbon nuclei based on ^{1}H–^{13}C heteronuclear multiple quantum coherence (HMQC) analyses. sc-XRD analyses[19] of **2a**–**2c** (Figure 1b) reveal the expected atom connectivity. The N1–C1–N2 bond angles (**2a** 111.9(1), **2b** 107.2(2), **2c** 106.7(1)°) and the N1–C1/N2–C1 bond lengths (**2a** 1.323(2)/1.333(2), **2b** 1.35(2)/1.349(2), **2c** 1.352(2)/1.353 (2) Å) are consistent with the related 1,3-imidazoli(ni)um cations.[13]

The CVs of C2-monophenylated salts (**IV-Ar**, Ar = Ph or 4-Tol)[15] show only a single 1e-reversible reduction process that corresponds to the redox couple **IV-Ar**/**VI** or **VII** (Scheme 1). In strong contrast, the CVs of the C2-

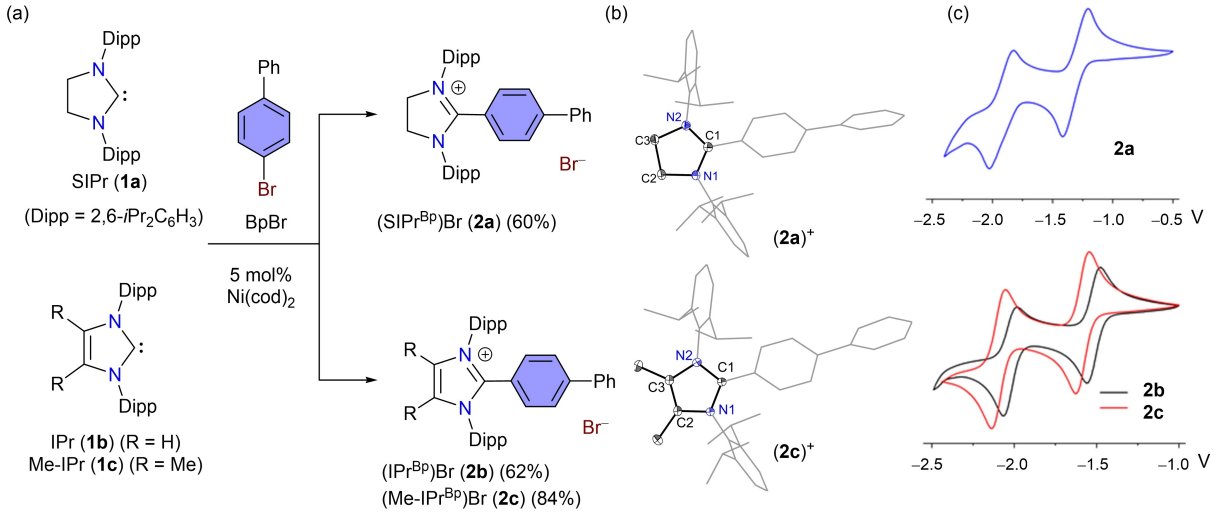

Figure 1. (a) Synthesis of C2-biphenylated 1,3-imidazoli(ni)ium salts **2a–2c**.(b) Solid-state molecular structures of **2a** and **2c**, only the cationic part is shown. Hydrogen atoms are omitted and the aryl substituents are shown as wire-frames for clarity. Thermal ellipsoids are drawn at the 50% probability. (c) Cyclovoltammograms (CVs) of **2a–2c** (in CH_3CN/ 0.1 M nBu_4NPF_6, 100 mV s^{-1}, vs Fc^+/Fc).

biphenylated species **2a**, **2b**, and **2c** (Figure 1c) exhibit two well-separated 1e-reversible redox processes in the negative potential region of −0.5 to −2.5 V (vs. Fc/Fc^+). The first reduction potential ($E_{1/2}$) for **2a** (−1.3 V), **2b** (−1.4 V), and **2c** (−1.6 V) each is consistent with the corresponding neutral mono-radicals. They are, however, at slightly lower negative potential than those of monophenylated derivatives $(SIPr^{Ph})Br$ (−1.4 V) and $(IPr^{Ph})Br$ (−1.7 V).[15] Treatments of **2a**, **2b**, and **2c** with KC_8 lead to the formation of radicals **3a** (blue), **3b** (green), and **3c** (green) as stable crystalline solids, respectively (Scheme 2). The appearance of the second reversible redox wave at $E_{1/2} = -1.9$ V (**2a**), −2.0 V (**2b**), and −2.1 V (**2c**) is remarkable and suggests the feasibility of further reduction of the radicals **3a–3c** into the anions.[20] Treatment of a blue (or green) THF solution of **3a** (or **3b**/**3c**) with KC_8 leads to the clean formation of the anion **4a-K** (or **4b-K**/**4c-K**) as a violet solid. The accessibility as well as the identity of the neutral radicals **3a–3c** and anions $(\mathbf{4a–4c})^-$ has also been corroborated by spectroelectrochemical (SEC) studies (see the Supporting Information).

The radicals **3a–3c** are stable in solutions as well as in the solid-state under an inert gas atmosphere and have been characterized by UV/Vis, EPR spectroscopy, and sc-XRD

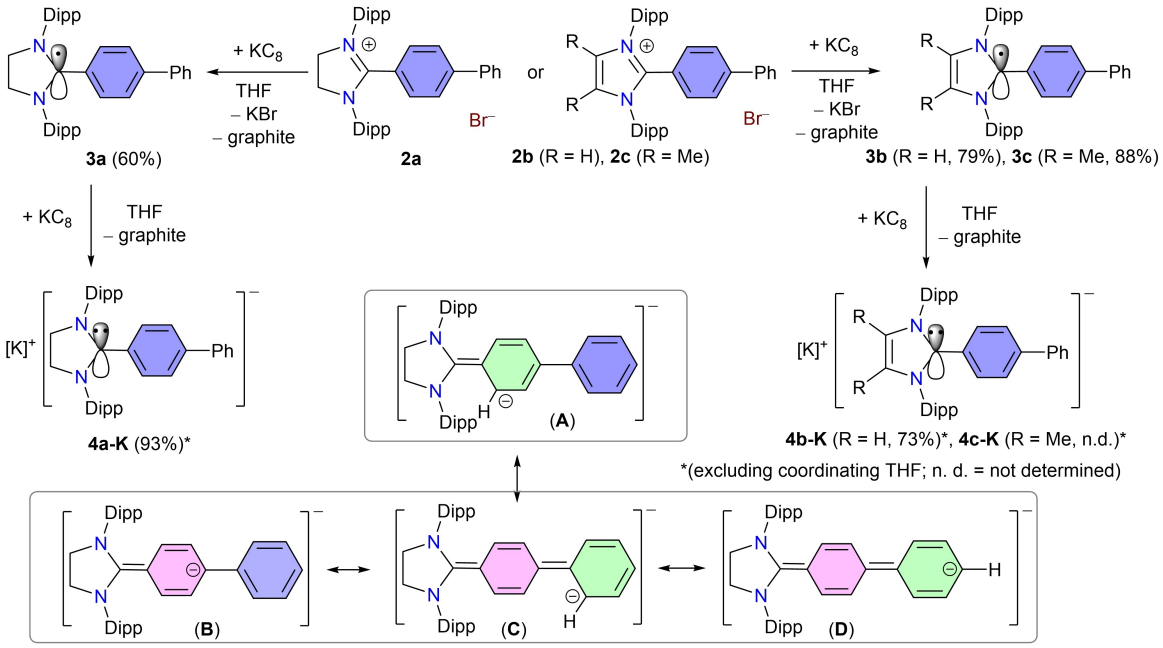

Scheme 2. Synthesis of radicals **3a–3c** and anions **4a-K–4c-K**. Selected resonance forms **A-D** of the anion $(\mathbf{4a})^-$.

(Figure 2). Note, unlike **3b** and **3c**, previously reported radicals **VI** (Scheme 1) based on an unsaturated NHC (i.e. IPr)[15] slowly decayed in solutions and hence could not be characterized by sc-XRD.[21] Thus, the use of a biphenyl substituent at the C2-position of NHCs enhances the stability of derived radicals by providing an additional room for the delocalization of the unpaired electron.[11] The anions **4a-K**–**4c-K** are extremely reactive and slowly decay in THF to partly form the corresponding radicals **3a**–**3c**, leading to the broadening of NMR signals. Remarkably, freshly prepared THF solutions of **4a-K** and **4b-K** containing a small pinch of KC_8 (≈1 mg for 0.5 mL solution) exhibited well-resolved sharp ^1H and ^{13}C NMR signals, suggesting their diamagnetic property. This approach was unfortunately not successful for **4c-K**, presumably due to its slightly higher reducing property (−2.1 V) than **4a-K**/**4b-K** (−1.9/−2.0 V). The ^1H NMR spectra of **4a-K** and **4b-K** show expected signals for the biphenyl (p-$C_6H_4C_6H_5$) moiety, which are high-field shifted compared to those of **2a** and **2b**. The high-field shifting of the Bp protons of **4a-K** and **4b-K** may be rationalized considering the delocalization of the electron lone-pair over the Bp-group as shown with the resonance structures **A-D** (Scheme 2). This is further corroborated by DFT calculations (see below).

Single crystals of the radicals **3a**, **3b**, and **3c** for sc-XRD were obtained on storing a saturated *n*-hexane solution of each at −32 °C. The solid-state molecular structures of **3a**, **3b**, and **3c** are shown in Figure 2. As previously observed for the mono-radicals **VII** (R′ = H, Scheme 1),[15] the C1–C4 (1.402(1) Å) and C1–N1/N2 (1.388(1)/1.398(1) Å) bond lengths are longer while the N1–C1–N2 (108.1(1)°) bond angle is more acute for **3a** with respect to those of **2a** (Table 1). The C1–C4 (1.402(1) Å) and C7–C8 (1.41(2) Å) bond lengths of **3a** are shorter than **2a** (1.471(2), 1.481(2) Å, respectively). Moreover, the bond length alteration (BLA) for the C–C bonds of the Bp-rings in **3a** (0.05–0.08 Å) is larger than that of **2a** (0.01 Å). These features indicate the delocalization of the unpaired electron over the C2-biphenyl unit, which accounts for the remarkable thermal stability of the radicals **3a**–**3c**. Similar trend in the structural parameters (C1–C2, C1–N1/N2 bond lengths, N1–C1–N2 bond angle, and BLA in Bp rings) of **3b** and **3c** is observed (see the Supporting Information for details). It is worth mentioning that the radicals **VI** (Scheme 1) based on an unsaturated NHC (i.e. IPr or Me-IPr) containing a mono-phenylated (Ar = Ph, 4-Tol or 4-$Me_2NC_6H_4$) C2-substituent have limited thermal stability and undergo bond activation on storage of their solutions at room temperature to form oxidized products (see Scheme S1 for an example).[15] This may be rationalized as the formation of **VI** (7π electron C_3N_2-ring) from **IV-Ar** (6π-electron planar C_3N_2-ring) occurs at the expense of aromaticity. This is not the case with SIPr-based radicals **VII** featuring a non-planar C_3N_2-ring. The presence of an additional phenyl ring in **3b** and **3c** provides an extra room for the delocalization of the unpaired electron and hence contributes to their stability. This is also in line with the spin-density distribution in **3a**–**3c** (see below).

For **4a-K**, single crystals suitable for sc-XRD were obtained by storing a saturated *n*-heptane solution of **4a-K** at 4 °C for four days. The molecular structure of **4a-K** has C_i symmetry featuring a hexameric cyclic structure with four THF molecules, i.e. $[(\mathbf{4a\text{-}K})_3(THF)_2]_2$ (Figure 3). Two potassium atoms bear a THF molecule, while one potassium coordinates with the *ortho*- and *ipso*-carbons of the biphenyl substituent of two $(\mathbf{4a})^-$ anions. The potassium atom coordinated by THF has close contacts with the aryl-carbon atoms of a Dipp substituent. Thus, each of the potassium atoms is formally eight-coordinated. The C1–C4, C40–C43, and C79–C82 bond lengths (av. 1.366(2) Å) of **4a-K** are shorter than the corresponding bonds of **2a** (1.471(2) Å) and **3a** (1.402(1) Å), indicating a considerable double bond character (see below for NBO analyses). This suggests that the negative charge in **4a-K** is mostly located at the *o*,*o*′ and *p*,*p*′-carbon atoms of the biphenyl group (see resonance structures **A-D**, Scheme 2), which is consistent with computational calculations (see below). All three potassium atoms have close contacts with the *o*,*o*′,*p*,*p*′-carbon atoms of the biphenyl substituents. The C–K interatomic distances range from 2.911(1) to 3.522(1) Å, which are shown as broken lines in Figure 3. As expected, the BLA for the Bp rings of **4a-K** (0.03–0.08 Å), like in **3a** (0.05–0.08 Å), is larger than that of **2a** (0.01 Å).

The optimized structures of **3a**–**3c** (Figures S35) at the BP86-D3(BJ)/def2-SVP as well as at the BP86-D3(BJ)/def2-TZVP level of theory are in good agreement with those determined by sc-XRD (Figure 2). The calculated natural partial charges (NPAs) for **3a**–**3c** (Table 2, Table S6) suggest that the Bp moiety is negatively charged by −0.31 (**3a**), −0.35(**3b**), and −0.38 (**3c**) with the first ring bearing the major part of the negative charge (see Figure S39). The

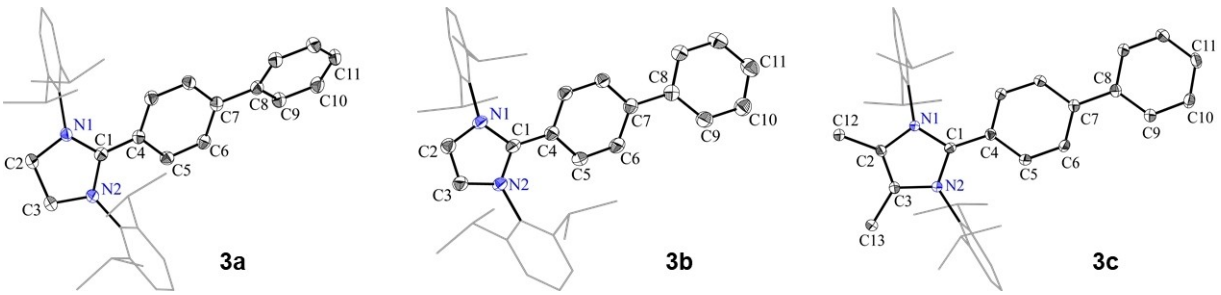

Figure 2. Solid-state molecular structures of radicals **3a**, **3b**, and **3c**. Hydrogen atoms are omitted and Dipp groups are shown as wireframes. Thermal dispacement ellipsoids are drawn at the 50% probability level.

Table 1: Selected experimental [and calculated at BP86-D3(BJ)/def2-SVP] bond lengths and bond angles of **2a**, **3a**, and $(\mathbf{4a})^-$. For $(\mathbf{4a})^-$, the values are given only for one of the three moieties of $[(\mathbf{4a\text{-}K})_3(THF)_2]_2$ (Figure 3).

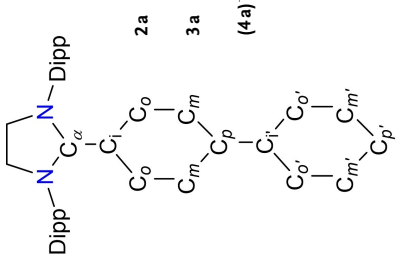

		C_α–C_i	C_i–C_o	C_o–C_m	C_m–C_p	C_p–$C_{i'}$	$C_{i'}$–$C_{o'}$	C_o–$C_{m'}$	C_m–$C_{p'}$
2a		1.471(2) [1.461]	1.399(2) 1.399(2)	1.381(2) 1.388(2)	1.399(2) 1.399(2)	1.481(2) [1.479]	1.398(2) 1.402(2)	1.385(2) 1.387(3)	1.384(3) 1.387(3)
			[1.415]	[1.394]	[1.417]		[1.416]	[1.401]	[1.405]
3a		1.402(1) [1.419]	1.431(1) 1.430(1)	1.368(1) 1.373(1)	1.414(1) 1.412(2)	1.469(1) [1.472]	1.406(2) 1.403(1)	1.386(1) 1.385(2)	1.388(2) 1.386(2)
			[1.438]	[1.387]	[1.425]		[1.421]	[1.400]	[1.406]
$(\mathbf{4a})^-$		1.366(2) [1.396]	1.460(2) [1.457]	1.366(2) [1.383]	1.433(2) [1.434]	1.440(2) [1.454]	1.424(2) [1.434]	1.378(2) [1.397]	1.398(2) [1.411]
		{1.389}[a]	{1.459}[a]	{1.377}[a]	{1.448}[a]	{1.449}[a]	{1.438}[a]	{1.397}[a]	{1.406}[a]

[a] within the hexamer $[(\mathbf{4a\text{-}K})_3(THF)_2]_2$, see Figure 3.

EPR spectrum of **3a** (Figure 4a, see the Supporting Information for **3b** and **3c**) measured at 298 K in THF exhibits a characteristic doublet signal. The EPR spectra of **3a**–**3c** were successfully simulated using calculated coupling constants (Table S12). The hyperfine coupling constants (*hfc*) are in good agreement with those calculated for **VI** and **VII**.[15] The singly occupied molecular orbitals (SOMOs) of **3a**–**3c** (Figure 4b, Figure S37) reveal an out-of-phase combination of the *p*-orbital at C_α with the adjacent nitrogen lone pair orbitals, while there is an in-phase combination between the *p*-orbital of C_α and C_i, which is in good agreement with the C_α–C_i double bond character (Wiberg Bond Index = 1.27e). Strikingly, there is a strong conjugation within the biphenyl substituent. Indeed, the plots of Mulliken spin densities for **3a**–**3c** (Figure 4c, Figure S38) show that the unpaired electron is mostly localized at the carbene carbon atom (27–39 %) and the *para*-C atom (26–27 %) of the first benzene ring. Interestingly, ≈15 % of the radical electron are located on the C_{ortho} and C_{para} atoms of the terminal phenyl ring. This number shows the electron withdrawing effect of the *para*-phenyl substituent at the C_6H_4-ring, enhancing the overall stability of the C2-biphenylated radicals **3a**–**3c** as well as introducing the possibility of hosting an additional electron into the SOMO to give stable anions $(\mathbf{4a}\text{–}\mathbf{c})^-$. Notably, the SOMOs of **3a** (−2.81 eV) and **3b** (−2.61 eV) are lower in energy than the corresponding C2-phenylated radicals **VII** (−2.67 eV) and **VI** (−2.40 eV).[15] The UV/Vis spectra of **3a**–**3c** (Figure 4d, Figure S19–S21) show three main absorption bands (λ_{max} (in nm) = 314, 393, 637 (**3a**); 301, 438, 684 (**3b**), 308, 406, 679 (**3c**)). According to TD-DFT studies (Tables S9–S11), these absorption bands of **3a** are related to HOMO-1→LUMO + 1, HOMO→LUMO + 5, and HOMO→LUMO transitions, respectively (HOMO = highest occupied molecular orbital; LUMO = lowest unoccupied molecular orbital). Based on TD-DFT analyses (Table S12–S14), the UV/Vis absorption bands (λ_{max} (in nm) = 294, 400, and 600 nm) in the SEC spectrum of the anion $\mathbf{4a}^-$ (Figure 4d) are related to HOMO-1→LUMO, HOMO→LUMO + 5/LUMO + 8, and HOMO→LUMO, respectively (see the Supporting Information for $\mathbf{4b}^-$ and $\mathbf{4c}^-$).

To examine the electronic structures of **4a-K**–**4c-K**, we performed quantum-chemical calculations at the BP86-D3-(BJ)/def2-SVP level of theory for the anionic species $(\mathbf{4a}\text{–}\mathbf{4c})^-$ without the inclusion of the counter cation. The comparison with the computed $[(\mathbf{4a\text{-}K})_3(THF)_2]_2$ structure reveal similar bond lengths (Table 1). As stated above, 1e-reduction of **3a** to give **4a-K** leads to the elongation of the C1–N1/N2 and shortening of the C1–C4 bond lengths (Table 1). The NPA charges (Table 2) indicate that the negative charge is mostly located at the biphenyl moiety ($\mathbf{4a}^-$: −0.80 e, $\mathbf{4b}^-$: −0.74 e, $\mathbf{4c}^-$: −0.77 e). Thus, the anions $(\mathbf{4a}\text{–}\mathbf{4c})^-$ are stabilized by the delocalization of the electron lone-pair over the biphenyl ring. Calculations predict singlet ground state of the anions $(\mathbf{4a}\text{–}\mathbf{4c})^-$ (Table 3). This is consistent with their well-resolved NMR signals measured at room temperature (see above). We also examined the diradical character of the model species $(\mathbf{4aM}\text{–}\mathbf{4cM})^-$, in which the Dipp substituents of $(\mathbf{4a}\text{–}\mathbf{4c})^-$ are replaced by

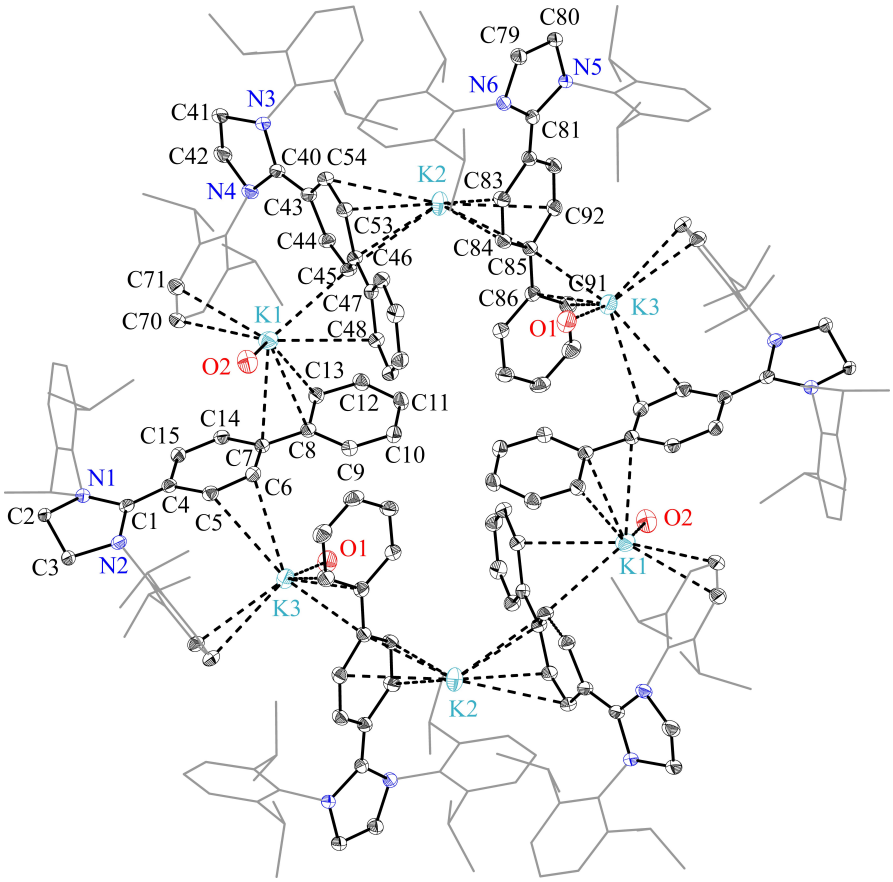

Figure 3. Solid-state molecular structure of $[(\mathbf{4a}\text{-}K)_3(THF)_2]_2$. Dipp groups are shown as wireframe models, H atoms and minor occupied disordered atoms have been omitted, and only the oxygen atom of THF is shown for clarity. Thermal dispacement ellipsoids are drawn at the 50% probability level. Symmetry code used: $1-x, 1-y, -z$.

Table 2: Selected NPA charges (Q) and WBIs of **2a**, **3a**, and $(\mathbf{4a})^-$.

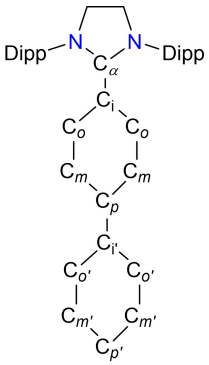

	NPA Charge (Q) C_α	N	Bp	$C_i/C_{i'}$	$C_o/C_{o'}$	C_m/C_m	$C_p/C_{p'}$
2a	0.51	−0.33	0.15	−0.16/−0.08	−0.16/−0.19	−0.20/−0.20	0.01/−0.19
3a	0.37	−0.41	−0.31	−0.18/−0.05	−0.22/−0.21	−0.20/−0.21	−0.08/−0.24
$(\mathbf{4a})^-$	0.23	−0.44	−0.80	−0.19/−0.04	−0.27/−0.24	−0.20/−0.22	−0.18/−0.31

	WBI N–C_α	C_α–C_i	C_i–C_o	C_o–C_m	C_m–C_p	C_p–$C_{i'}$	$C_{i'}$–$C_{o'}$
2a	1.29	1.10	1.34	1.48	1.36	1.09	1.37
3a	1.09	1.27	1.23	1.55	1.30	1.12	1.35
$(\mathbf{4a})^-$	1.00	1.42	1.16	1.61	1.25	1.20	1.29

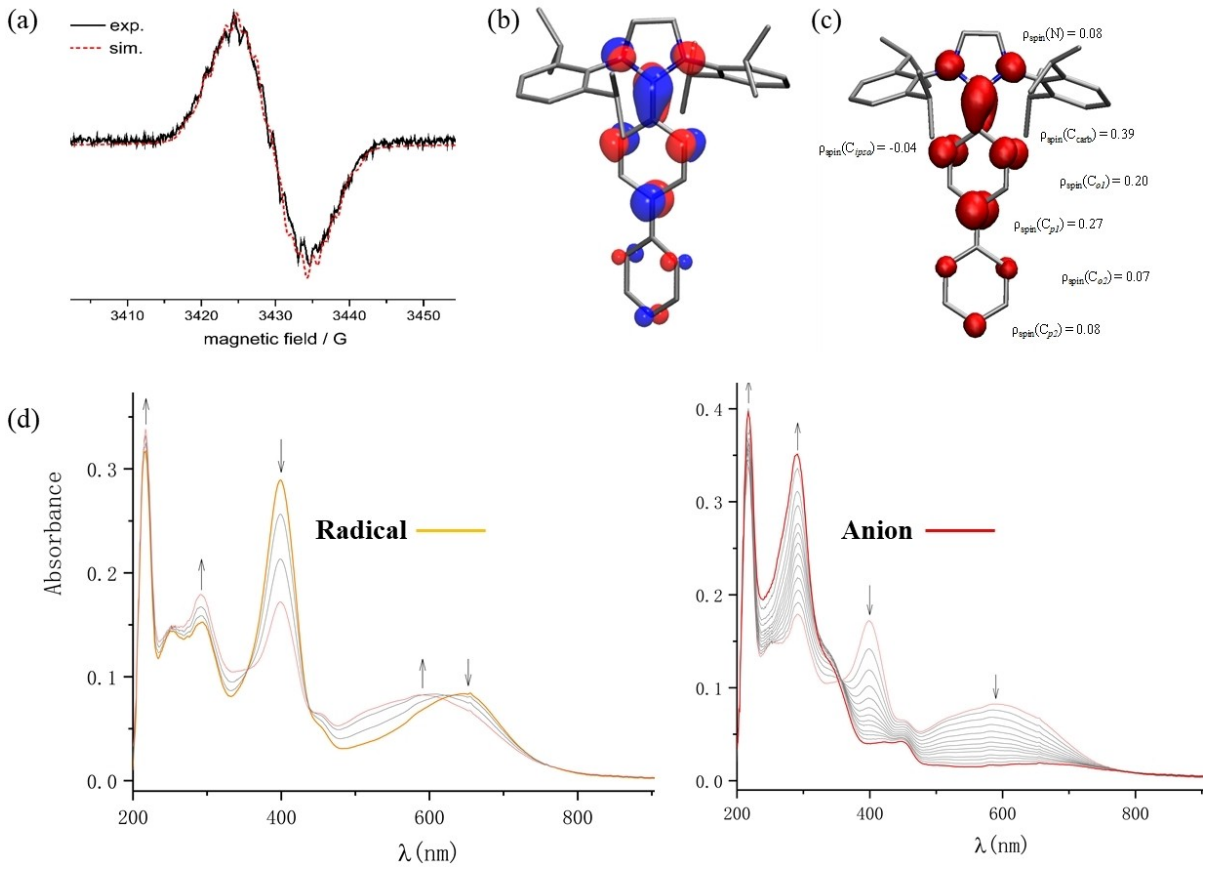

Figure 4. (a) X-Band continuous wave EPR spectrum in THF at 298 K (ν = 9.63 GHz, P_{mw} = 2 mW, Mod. Amp. 0.3 mT), (b) plot of the SOMO, and (c) Mulliken spin density distribution (isovalue 0.003 a.u.) for **3a**. (d) UV/Vis SEC (spectroelectrochemical) spectra of radical (**3a**) and anion (**4a**$^-$) recorded using **2a** in 0.1 M nBu$_4$NPF$_6$ in acetonitrile (see the Supporting Information for details).

Table 3: Singlet-triplet energy gap ($\Delta E_{S\text{-}T}$, in kcal mol^{-1}) for the anions (**4a–4c**)$^-$ and their model systems (**4aM–4cM**)$^-$ in which Dipp substituents were replaced by methyl groups.

Method	(**4a**)$^-$	(**4aM**)$^-$	(**4b**)$^-$	(**4bM**)$^-$	(**4c**)$^-$	(**4cM**)$^-$
B3LYP + D3(BJ)/def2-TZVPP[a]	24.0	34.1	19.5	26.1	16.9	28.6
PBE0 + D3(BJ)/def2-TZVPP[a]	25.0	35.3	20.0	25.7	17.2	30.6
M06-2X/def2-TZVPP[a]	32.2	40.9	25.6	33.5	22.7	35.4
CASSCF(12,12)/def2-TZVP	–	40.3	–	41.9	–	40.3
CASSCF + NEVPT2(12,12)/def2-TZVP	–	37.1	–	34.4	–	36.2

[a] Single point on the optimized geometry at BP86 + D3(BJ)/def2-SVP.

methyl groups, by CASSCF + NEVPT2(12,12) calculations. Our active space includes the most relevant biphenyl group. The CI vector has a contribution of 0.82 for the (222222000000) configuration and 0.03 for the (222220200000), which reveals a weak multiconfigurational nature of the anionic species (**4aM–4cM**)$^-$ (Table S8). The diradical character calculated with these values according to Bachler et al. amounts to 6.7 %.[22]

Efforts to obtain single crystals of **4b-K** were unsuccessful due to its slow decay in solutions to form **3b**. We attempted the synthesis of a compound featuring an organic cation by reacting **4b-K** with (Ph$_4$P)Cl. The reaction however led to the formation of radical **3b** and PPh$_3$ instead of the expected cation exchange product **4b-PPh$_4$** (Scheme 3). This suggests strong reducing property of (**4b**)$^-$ that induces P–C$_{Ph}$ bond cleavage of (Ph$_4$P)$^+$ to form **3b** and PPh$_3$ along with the C–C coupling product biphenyl (PhPh).[23] The degradation of (Ph$_4$P)$^+$ with lithium amides via free-radical pathways is literature known.[24] As expected, treatment of **4a-K** (or **4b-K**) with **2a** (or **2b**) cleanly affords **3a** (or **3b**). The reducing property of **3b** was further explored with Ph$_2$PCl and Ph$_2$P(O)Cl, which resulted in the homocoupling products (Ph$_2$P)$_2$ (^{31}P NMR = −14.9 ppm)[25] or (Ph$_2$P(O))$_2$ (^{31}P NMR = 26.6 ppm)[26] and the salt (**2b**)Cl. Treatment of **4a-K** with AgOTf leads to the clean formation of the radical **3a**, which further reacts with an additional AgOTf to give (**2a**)OTf (see Table S1 for the titration of **4a-K** with AgOTf).

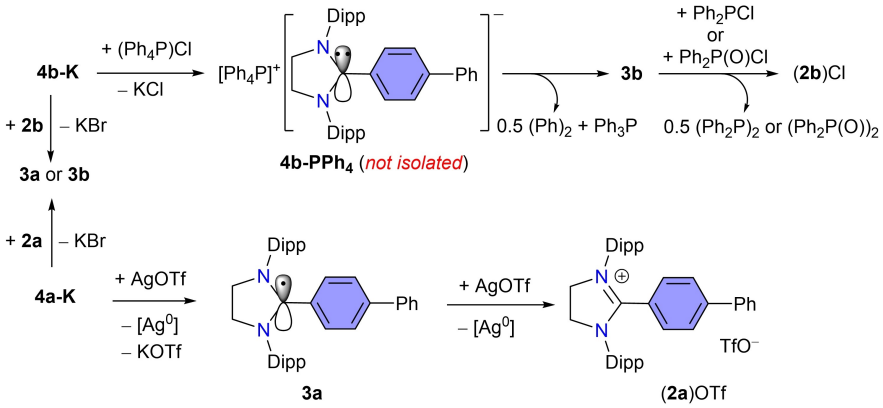

Scheme 3. Reaction of **4b-K** with $(Ph_4P)Cl$ to Ph_3P and **3b**. Reductive homocoupling of Ph_2PCl and $Ph_2P(O)Cl$ with **3b**. Reactions of **4a-K** and **3a** with AgOTf to **3a** and (**2a**)OTf, respectively.

Conclusion

In conclusion, the accessibility of three stable redox states has been shown with C2-biphenylated 1,3-imidazoli(ni)um salts **2a**–**2c**, which forms stable radicals **3a**–**3c** and anions **4a-K**–**4c-K** on sequential one-electron reduction with KC_8. The use of a biphenyl substituent at the C2-position of classical NHCs enhances the stability of the corresponding radicals (**3a**–**3c**) compared to mono-phenylated (Ar = Ph or substituted monoaryl) derivatives. Remarkably, this also introduces an additional stable redox state to the systems, the anions $(\mathbf{4a}–\mathbf{4c})^-$. The isolation of crystalline anions is unprecedented in the NHC chemistry. The radicals **3a**–**3c** have been characterized by EPR spectroscopy and sc-XRD. The anions **4a-K** and **4b-K** have been characterized by NMR spectroscopy and the solid-state molecular structure of **4a-K** has been established by sc-XRD. Reactivity studies of **3a**, **3b** and **4a-K**, **4b-K** towards Ph_2PCl, $Ph_2P(O)Cl$ and $(Ph_4P)Cl$ have been shown. The facile accessibility of **4a-K** and **4b-K** is expected to add new facets to the NHC as well as organometallic chemistry.

Acknowledgements

We are extremely grateful the Deutsche Forschungsgemeinschaft (DFG) for generous support (GH 129/4-2 and GH 129/9-1). The authors are thankful to Professor Norbert W. Mitzel for his continuous support. Open Access funding enabled and organized by Projekt DEAL.

Conflict of Interest

The authors declare no conflict of interest.

Data Availability Statement

The data that support the findings of this study are available in the supplementary material of this article.

Keywords: Carbanions · Carbenes · Multiple Redox-States · N-Heterocycle · Radicals

[1] K. V. Raman, A. M. Kamerbeek, A. Mukherjee, N. Atodiresei, T. K. Sen, P. Lazić, V. Caciuc, R. Michel, D. Stalke, S. K. Mandal, S. Blügel, M. Münzenberg, J. S. Moodera, *Nature* **2013**, *493*, 509–513.

[2] a) Y. Morita, S. Suzuki, K. Sato, T. Takui, *Nat. Chem.* **2011**, *3*, 197–204; b) S. Muench, A. Wild, C. Friebe, B. Häupler, T. Janoschka, U. S. Schubert, *Chem. Rev.* **2016**, *116*, 9438–9484; c) T. B. Schon, B. T. McAllister, P.-F. Li, D. S. Seferos, *Chem. Soc. Rev.* **2016**, *45*, 6345–6404; d) J. Winsberg, T. Hagemann, T. Janoschka, M. D. Hager, U. S. Schubert, *Angew. Chem. Int. Ed.* **2017**, *56*, 686–711; *Angew. Chem.* **2017**, *129*, 702–729; e) Y. Ding, C. Zhang, L. Zhang, Y. Zhou, G. Yu, *Chem. Soc. Rev.* **2018**, *47*, 69–103; f) P. Poizot, J. Gaubicher, S. Renault, L. Dubois, Y. Liang, Y. Yao, *Chem. Rev.* **2020**, *120*, 6490–6557.

[3] a) T. Nishinaga, *Organic Redox Systems: Synthesis, Properties, and Applications*, Wiley, Hoboken, **2016**; b) G. Schweicher, G. Garbay, R. Jouclas, F. Vibert, F. Devaux, Y. H. Geerts, *Adv. Mater.* **2020**, *32*, 1905909.

[4] a) Q. Peng, A. Obolda, M. Zhang, F. Li, *Angew. Chem. Int. Ed.* **2015**, *54*, 7091–7095; *Angew. Chem.* **2015**, *127*, 7197–7201; b) E. Neier, R. Arias Ugarte, N. Rady, S. Venkatesan, T. W. Hudnall, A. Zakhidov, *Org. Electron.* **2017**, *44*, 126–131; c) X. Ai, E. W. Evans, S. Dong, A. J. Gillett, H. Guo, Y. Chen, T. J. H. Hele, R. H. Friend, F. Li, *Nature* **2018**, *563*, 536–540; d) X. Hu, W. Wang, D. Wang, Y. Zheng, *J. Mater. Chem. C* **2018**, *6*, 11232–11242; e) H. Guo, Q. Peng, X.-K. Chen, Q. Gu, S. Dong, E. W. Evans, A. J. Gillett, X. Ai, M. Zhang, D. Credgington, V. Coropceanu, R. H. Friend, J.-L. Brédas, F. Li, *Nat. Mater.* **2019**, *18*, 977–984; f) E. Cho, V. Coropceanu, J.-L. Brédas, *J. Am. Chem. Soc.* **2020**, *142*, 17782–17786; g) P. Murto, H. Bronstein, *J. Mater. Chem. C* **2022**, *10*, 7368–7403.

[5] a) D. A. Wilcox, V. Agarkar, S. Mukherjee, B. W. Boudouris, *Annu. Rev. Chem. Biomol. Eng.* **2018**, *9*, 83–103; b) L. Ji, J. Shi, J. Wei, T. Yu, W. Huang, *Adv. Mater.* **2020**, *32*, 1908015.

[6] a) S. Sanvito, *Chem. Soc. Rev.* **2011**, *40*, 3336–3355; b) I. Ratera, J. Veciana, *Chem. Soc. Rev.* **2012**, *41*, 303–349; c) Z. Zeng, X. Shi, C. Chi, J. T. Lopez Navarrete, J. Casado, J. Wu, *Chem. Soc. Rev.* **2015**, *44*, 6578–6596; d) T. Y. Gopalakrishna, W. Zeng, X. Lu, J. Wu, *Chem. Commun.* **2018**, *54*, 2186–2199; e) Y. Huang, E. Egap, *Polym. J.* **2018**, *50*, 603–614.

[7] M. Newcomb, in *Reactive Intermediate Chemistry* (Eds.: R. A. Moss, M. S. Platz), Wiley, Hoboken, **2005**, p. 121–163.

[8] M. Gomberg, *J. Am. Chem. Soc.* **1900**, *22*, 757–771.

[9] R. G. Hicks, *Stable Radicals: Fundamentals and Applied Aspects of Odd-Electron Compounds*, Wiley, Hoboken, **2010**.
[10] a) Y. Kim, E. Lee, *Chem. Eur. J.* **2018**, *24*, 19110–19121; b) K. Kato, A. Osuka, *Angew. Chem. Int. Ed.* **2019**, *58*, 8978–8986; *Angew. Chem.* **2019**, *131*, 9074–9082; c) R. S. Ghadwal, *Synlett* **2019**, *30*, 1765–1775; d) H. Song, E. Pietrasiak, E. Lee, *Acc. Chem. Res.* **2022**, *55*, 2213–2223.
[11] a) J. K. Mahoney, D. Martin, C. E. Moore, A. L. Rheingold, G. Bertrand, *J. Am. Chem. Soc.* **2013**, *135*, 18766–18769; b) C. D. Martin, M. Soleilhavoup, G. Bertrand, *Chem. Sci.* **2013**, *4*, 3020–3030; c) J. Park, H. Song, Y. Kim, B. Eun, Y. Kim, D. Y. Bae, S. Park, Y. M. Rhee, W. J. Kim, K. Kim, E. Lee, *J. Am. Chem. Soc.* **2015**, *137*, 4642–4645; d) M. Soleilhavoup, G. Bertrand, *Acc. Chem. Res.* **2015**, *48*, 256–266; e) K. C. Mondal, S. Roy, H. W. Roesky, *Chem. Soc. Rev.* **2016**, *45*, 1080–1111; f) J. Back, J. Park, Y. Kim, H. Kang, Y. Kim, M. J. Park, K. Kim, E. Lee, *J. Am. Chem. Soc.* **2017**, *139*, 15300–15303; g) M. M. Hansmann, M. Melaimi, D. Munz, G. Bertrand, *J. Am. Chem. Soc.* **2018**, *140*, 2546–2554; h) J. Messelberger, A. Grünwald, P. Pinter, M. M. Hansmann, D. Munz, *Chem. Sci.* **2018**, *9*, 6107–6117; i) S. Kundu, S. Sinhababu, V. Chandrasekhar, H. W. Roesky, *Chem. Sci.* **2019**, *10*, 4727–4741; j) T. Ullrich, D. Munz, D. M. Guldi, *Chem. Soc. Rev.* **2021**, *50*, 3485–3518; k) Z. Feng, S. Tang, Y. Su, X. Wang, *Chem. Soc. Rev.* **2022**, *51*, 5930–5973; l) K. Breitwieser, H. Bahmann, R. Weiss, D. Munz, *Angew. Chem. Int. Ed.* **2022**, *61*, e202206390; *Angew. Chem.* **2022**, *134*, e202206390; m) R. S. Ghadwal, *Acc. Chem. Res.* **2022**, *55*, 457–470.
[12] a) I. McKenzie, J.-C. Brodovitch, P. W. Percival, T. Ramnial, J. A. C. Clyburne, *J. Am. Chem. Soc.* **2003**, *125*, 11565–11570; b) T. Ramnial, I. McKenzie, B. Gorodetsky, E. M. W. Tsang, J. A. C. Clyburne, *Chem. Commun.* **2004**, 1054–1055.
[13] R. S. Ghadwal, S. O. Reichmann, R. Herbst-Irmer, *Chem. Eur. J.* **2015**, *21*, 4247–4251.
[14] a) D. Rottschäfer, C. J. Schürmann, J.-H. Lamm, A. N. Paesch, B. Neumann, R. S. Ghadwal, *Organometallics* **2016**, *35*, 3421–3429; b) N. K. T. Ho, B. Neumann, H.-G. Stammler, V. H. Menezes da Silva, D. G. Watanabe, A. A. C. Braga, R. S. Ghadwal, *Dalton Trans.* **2017**, *46*, 12027–12031; c) A. Merschel, D. Rottschäfer, B. Neumann, H.-G. Stammler, R. S. Ghadwal, *Organometallics* **2020**, *39*, 1719–1729; d) D. Rottschäfer, T. Glodde, B. Neumann, H. G. Stammler, R. S. Ghadwal, *Chem. Commun.* **2020**, *56*, 2027–2030; e) A. Merschel, T. Glodde, B. Neumann, H.-G. Stammler, R. S. Ghadwal, *Angew. Chem. Int. Ed.* **2021**, *60*, 2969–2973; *Angew. Chem.* **2021**, *133*, 3006–3010.
[15] D. Rottschäfer, B. Neumann, H.-G. Stammler, M. V. Gastel, D. M. Andrada, R. S. Ghadwal, *Angew. Chem. Int. Ed.* **2018**, *57*, 4765–4768; *Angew. Chem.* **2018**, *130*, 4855–4858.
[16] a) P. Wei, J. H. Oh, G. Dong, Z. Bao, *J. Am. Chem. Soc.* **2010**, *132*, 8852–8853; b) B. D. Naab, S. Guo, S. Olthof, E. G. B. Evans, P. Wei, G. L. Millhauser, A. Kahn, S. Barlow, S. R. Marder, Z. Bao, *J. Am. Chem. Soc.* **2013**, *135*, 15018–15025.
[17] A. Das, J. Ahmed, N. M. Rajendran, D. Adhikari, S. K. Mandal, *J. Org. Chem.* **2021**, *86*, 1246–1252.
[18] Radicals **VI** based on an unsaturated NHC were found to have a shorter half-life in solution with respect to those derived from a saturated NHC (SIPr). See the Supporting Information for details.
[19] Details of the X-ray diffraction are given in the Supporting Information. Deposition numbers 2208077 (**2a**), 2208078 (**2c**), 1947129 (**3a**), 1947127 (**3b**), 1947128 (**3c**), and 2208079 (**4a-K**) contain the supplementary crystallographic data for this paper. These data are provided free of charge by the joint Cambridge Crystallographic Data Centre and Fachinformationszentrum Karlsruhe Access Structures service.
[20] Formation of a carbene on deprotonation of an 1,3-imidazolium salt is a formal two electron redox process.
[21] See the Supporting Information for a possible decomposition product of **VI**, which has been identified by sc-XRD.
[22] V. Bachler, G. Olbrich, F. Neese, K. Wieghardt, *Inorg. Chem.* **2002**, *41*, 4179–4193.
[23] M. Zhou, T. Qin, in *Free Radicals: Fundamentals and Applications in Organic Synthesis 2, Vol. 2020/5*, Georg Thieme, Stuttgart, **2021**.
[24] O. A. Rebrova, N. A. Nesmeyanov, V. V. Mikul′shina, O. A. Reutov, *Bull. Acad. Sci. USSR Div. Chem. Sci.* **1975**, *24*, 326–329.
[25] V. P. W. Böhm, M. Brookhart, *Angew. Chem. Int. Ed.* **2001**, *40*, 4694–4696; *Angew. Chem.* **2001**, *113*, 4832–4834.
[26] J. E. Nycz, R. Musiol, *Heteroat. Chem.* **2006**, *17*, 310–316.

Manuscript received: October 18, 2022
Accepted manuscript online: November 18, 2022
Version of record online: December 22, 2022